Optics Letters

Intra-pulse difference-frequency generation of mid-infrared (2.7–20 μm) by random quasi-phase-matching

Jinwei Zhang,[1,†] Kilian Fritsch,[2,†] Qing Wang,[1,3,†] Ferenc Krausz,[1,2] Ka Fai Mak,[1,*] and Oleg Pronin[1]

[1]Max-Planck Institute of Quantum Optics, Hans-Kopfermann-Str. 1, 85748 Garching, Germany
[2]Ludwig-Maximilians Universität München, Am Coulombwall 1, 85748 Garching, Germany
[3]School of Optics and Photonics, Beijing Institute of Technology, 100081 Beijing, China
*Corresponding author: k.mak@physik.uni-muenchen.de

Received 1 March 2019; revised 1 May 2019; accepted 16 May 2019; posted 16 May 2019 (Doc. ID 361268); published 5 June 2019

We present a mid-infrared (MIR) source based on intra-pulse difference-frequency generation under the random quasi-phase-matching condition. The scheme enables the use of non-birefringent materials whose crystal orientations are not perfectly and periodically poled, widening the choice of media for nonlinear frequency conversion. With a 2 μm driving source based on a Ho:YAG thin-disk laser, together with a polycrystalline ZnSe element, an octave-spanning MIR continuum (2.7–20 μm) was generated. At over 20 mW, the average power is comparable to regular phase-matching in birefringent crystals. A 1 μm laser system based on a Yb:YAG thin-disk laser was also tested as a driving source in this scheme. The new approach provides a simplified way for generating coherent MIR radiation with an ultrabroad bandwidth at reasonable efficiency.

https://doi.org/10.1364/OL.44.002986

Coherent mid-infrared (MIR) light has a plethora of important applications ranging from life sciences to industrial processes. Due to the presence of many molecular "finger-print" absorption features in this spectral region, a simultaneous coverage of this range will enable the parallel detection and identification of a vast number of chemicals [1,2]. This wavelength range can be covered by numerous different schemes, each with their own strengths and weaknesses in terms of complexity, simultaneous bandwidth, power, efficiency, and pulse durations [3–8]. Yet, the most popular method of coherent broadband MIR generation remains nonlinear downconversion from the near-infrared—a spectral region where many high-power driving lasers are available [4,7,9–18]. Obviously, this process requires a suitable nonlinear medium that is transparent for the pump, signal, and idler wavelengths. Furthermore, for effective conversion, phase-matching between the beams is crucial. This is usually achieved by birefringent crystals placed at specific angles to the beam [4,10,12]. Quasi-phase-matching (QPM) is also often employed with non-birefringent crystals, where the crystal orientation is periodically inverted to substantially enhance the generated signal [7,19].

Random QPM (RQPM) [20] is an alternative approach which has recently been demonstrated in an optical parametric oscillator (OPO) [21]. The nonlinear medium is an aggregate of randomly oriented single-crystal grains that are tens of micrometers in size. Instead of a periodic reversal of crystal axis as in the case of ideal QPM, the crystal axis changes randomly along the beam path. Yet, the nonlinear susceptibility and the corresponding signal do not average to zero [20]. The result is a gradual growth of the generated signal linear to the propagation length. Consequently, non-birefringent materials whose crystal orientation cannot easily be manipulated for QPM can still be used. Though much lower in efficiencies compared to commonly used phase-matching schemes, RQPM offers an unparalleled phase-matching bandwidth that is insensitive to the incident angle. In addition, unlike single crystals, polycrystals can easily be grown to larger dimensions to enable longer interaction lengths [22].

The scheme was first demonstrated to generate a tunable difference-frequency generation (DFG) signal in the MIR by mixing two nanosecond lasers [20]. To exploit the full phase-matching bandwidth simultaneously and generate a broadband MIR continuum, an ultrashort pump pulse can also be used. Using the components within a single-broadband pulse (intra-pulse) for DFG can also result in the canceling of carrier-envelope phases (CEP), giving rise to intrinsically CEP-stable MIR output [4,10]. However, to generate a meaningful amount of signal, a high pump power is required.

The needed high power has recently been achieved within the cavity of an OPO, which resulted in a broadband MIR continuum spanning from 3 to 7.5 μm [21]. Though successful, an OPO requires the alignment of two cavities at interferometric precision, which increases the complexity of the system. RQPM has also recently been demonstrated inside the cavity of a femtosecond polycrystalline Cr:ZnS oscillator and in a single-pass amplifier operating at 2400 nm, generating sum-frequency signals and broadband second and fourth harmonics down

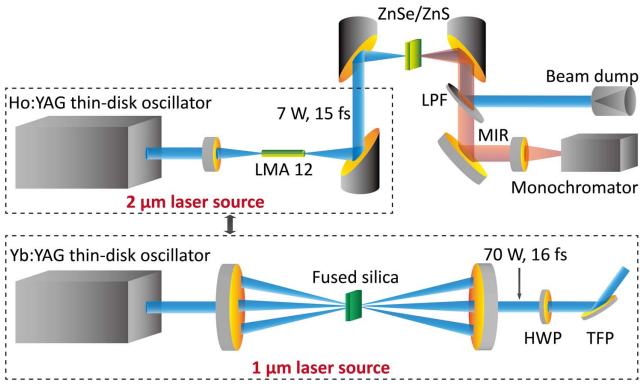

Fig. 1. Experimental setup. A Ho:YAG-based 2 μm laser source and a Yb:YAG-based 1 μm laser source are separately tested for driving intra-pulse DFG in polycrystalline ZnSe/ZnS. LPF, long-pass filter; HWP, half-wave plate; TFP, thin-film polarizer.

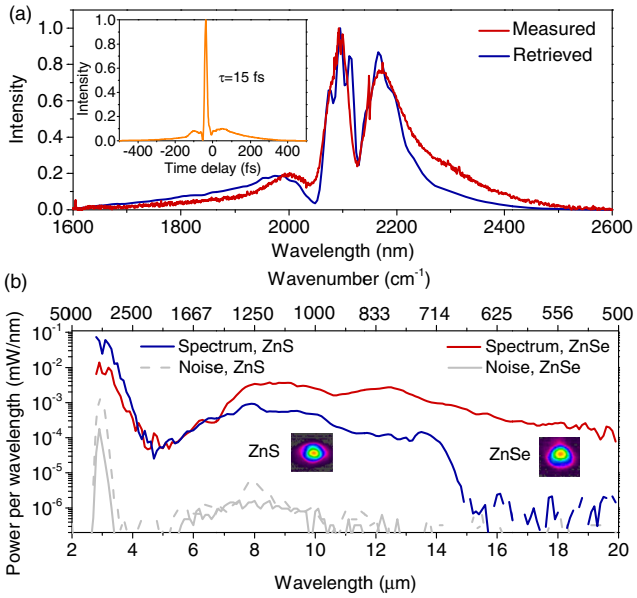

Fig. 2. (a) Characterization of the 2 μm driving pulses. Red line, measured spectrum by a Fourier transform infrared (FTIR) spectrometer (Bristol 721); blue line, retrieved spectrum from a home-built second-harmonic frequency-resolved optical gating (FROG); inset, retrieved temporal intensity by FROG, indicating a pulse duration of 15 fs. (b) MIR spectra with ZnSe crystal and ZnS crystal pumped by a 2 μm laser source. The measured average output powers are 16 and 22 mW, respectively, behind the 2.7 μm long-pass filter. The beam profiles of the MIR beam are measured by a beam profiling camera (Pyrocam-III Ophir). The noise floors or background spectra are measured with the nonlinear crystals shifted by ∼1 mm away from the focus.

to 510 nm [23,24]. In this Letter, we describe the use of a Ho:YAG thin-disk oscillator lasing at 2 μm, in combination with a fiber pulse-compressor, as a high-power femtosecond driver for intra-pulse DFG towards the longer wavelengths based on RQPM. The method, relying on a single-beam geometry, provides an octave-spanning MIR continuum (2.7-20 μm) at over 20 mW of average power. This power level and the corresponding brightness already match those available from synchrotron infrared beam lines [3]. A 1 μm system based on a Yb:YAG thin-disk laser and a multi-pass compression system were also tested as the driving source in this scheme, which shows much lower efficiencies.

The experimental setup is shown in Fig. 1. The initial pulses are produced by a Kerr-lens mode-locked Ho:YAG thin-disk oscillator that operates at a repetition rate of 77 MHz [25]. The oscillator delivers 260 fs pulses at 2.1 μm with an average power of 18 W. A temporal self-compression down to 15 fs [Fig. 2(a)] with an average power of 7 W is achieved in a commercial silica-core photonic-crystal fiber [12]. The central wavelength of this driving source corresponds to a low photon energy of 0.6 eV, mitigating multiphoton absorption in the nonlinear crystal and enabling a high-power operation of the intra-pulse DFG scheme.

Among the many disordered polycrystalline materials, ZnSe is one of the most suitable candidates to generate MIR via intra-pulse DFG due to its broad transparency in the MIR range (0.55 to 20 μm) and relatively high nonlinearity ($d_{14} = 20$ pm/V). In addition, compared to other nonlinear crystals, it has a high optical damage threshold and high thermal conductivity, and is readily available commercially. Another promising candidate is ZnS, which has very similar properties as ZnSe, except for its narrower transparency window (0.55–15 μm). Both polycrystalline materials are used in this Letter to generate MIR radiation via RQPM with our recently developed femtosecond Ho:YAG thin-disk laser source [12,25].

The self-compressed pulses are focused, using a gold-coated off-axis parabolic mirror, into a 2-mm-thick ZnSe crystal to a spot diameter of 60 μm. The crystal has a grain size of 50–70 μm according to the vendor (Edmund Optics), which is not far from the ∼75 μm DFG coherence length in ZnSe crystal driven by a 1.9 μm pump and 2.3 μm signal [26]. The crystal is placed at an incident angle of 15° to reduce back-reflection into the laser system. Unlike regular birefringent crystals, random phase-matching in a polycrystalline element does not require a specific crystal orientation or input beam polarization. Due to the high reflection loss of the uncoated ZnSe, only 5.6 W of light entered the crystal, corresponding to a peak intensity of 110 GW/cm^2 when the pulse's temporal pedestal is taken into account. The generated MIR radiation was separated from the transmitted driving beam by a long-pass filter and sent to a monochromator (Newport Cornerstone 260) for spectral measurement. To suppress second-order diffractions from the monochromator's grating, four long-pass filters with cut-on wavelengths at 2.7, 4.5, 7.3, and 11 μm were used to record four different spectra spanning from 2.7 to 5.5 μm, 4.5 to 8.5 μm, 6 to 13 μm, and 10 to 22 μm. The intensities of the measured spectra have been calibrated using a silicon nitride infrared emitter (Bentham Instruments Ltd). This corrects for losses in the long-pass filters and the ZnSe lens used to focus light into the monochromator, and the low dispersion efficiency of the monochromator grating at longer wavelengths (starting from 11 μm). The corrected spectra were then stitched together to produce the final spectrum.

As shown in Fig. 2(b), the spectrum spans nearly three octaves and covers the wavelength range from 2.7 to 20 μm (at −30 dB)—a bandwidth that can support few-cycle pulses in the MIR. Interestingly, a cascaded intra-pulse difference-frequency process is also found under the RQPM condition [15,16].

This process generates an ultra-broadband MIR spectrum, even with significantly narrower input bandwidth. Via the standard intra-pulse DFG process, the MIR spectrum would have only reached down to 4.5 μm instead of 2.7 μm achieved in this Letter. An average power of 16 mW was measured (S302C, Thorlabs) behind a long-pass filter with a cut-on wavelength of 2.7 μm. Taking into account the >10% loss of the long-pass filter above 2.7 μm and the reflection loss on the uncoated ZnSe crystal surface, we conclude that the generated MIR power inside the crystal reached 25 mW. The reflection loss can potentially be reduced by applying an appropriate anti-reflection coating. The beam profile of the MIR is shown in Fig. 2(b). The MIR beam exhibits the same polarization as the incident fundamental laser beam. The MIR average power was recorded for 1 h, showing power fluctuations of approximately 6% (root mean square). This large fluctuation originates from the limited optimization of the mechanical stability of the oscillator and the fiber compression stage. A significantly better stability for the MIR output can be expected when a robust laser housing and a thermally-stabilized fiber holder are used.

After exchanging the ZnSe crystal with a 2 mm thick ZnS crystal, we also observed MIR generation and the cascaded intra-pulse DFG process. A spectral coverage spanning from 2.7 to 15 μm was obtained, as shown in Fig. 2(b). An average power of 22 mW was measured behind the 2.7 μm long-pass filter, corresponding to an average power of 35 mW generated inside the crystal. The grain size for the ZnS crystal is estimated to be ~60 μm, according to the manufacturer (Korth Kristalle GmbH), close to the coherence length of ~55 μm [27]. We believe this better matching of the coherence length, as compared to the ZnSe case, led to the improved conversion efficiency.

As a comparison, a 1 μm laser system based on a Yb:YAG thin-disk oscillator was also used as the driving source to generate MIR via RQPM. The system can deliver 16 fs pulses [Fig. 3(a)] with an average power of 70 W at a repetition rate of 28 MHz. The configuration of this system is very similar to the one published by Fritsch *et al.* [28], but with only two Herriott cells for the spectral broadening instead of three. Both ZnSe and ZnS crystals were tested under an average input power of 4 and 6.5 W, respectively. They correspond to intensities of 56 and 90 GW/cm^2 for a larger spot diameter of 120 μm, taking into account the reflection loss from the surface of the crystals. These intensities are in each case just below the damage threshold, which is defined to be the minimum power needed to repeatedly induce damage at five different locations on a given crystal. In comparison, with a 2 μm driving source, no crystal damage was found, even at the maximum input power of 7 W with the corresponding peak intensity of 110 GW/cm^2 inside the crystal. The lower damage threshold when pumping at the 1 μm wavelength can be attributed to the increased multiphoton absorption at higher photon energies [29,30].

The generated MIR has an average power of 0.3 and 0.5 mW, respectively, measured behind the 2.7 μm long-pass filter. The generated MIR power inside the crystals can be calculated as 0.5 and 0.8 mW, respectively. The measured spectra are shown in Fig. 3(b). The corresponding conversion efficiencies are more than 20 times lower compared to the case with the 2 μm driving source. These values are summarized in Table 1. The first reason for the lower efficiency is the lower damage

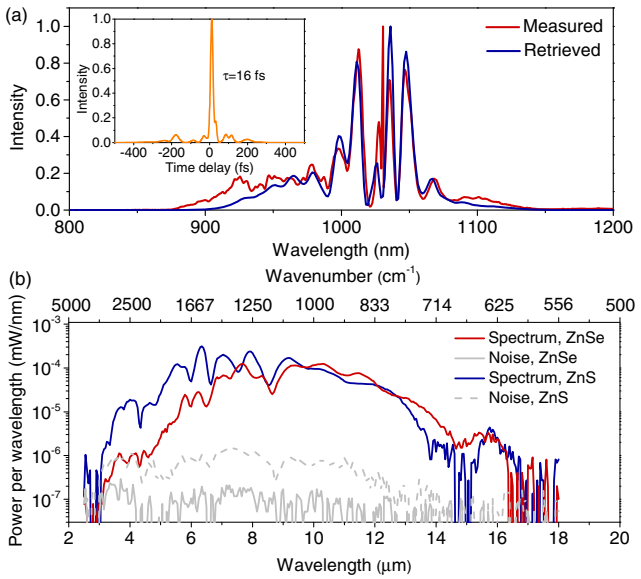

Fig. 3. (a) Characterization of the 1 μm driving pulses. Red line, measured spectrum by an optical spectrum analyzer (Yokogawa); blue line, retrieved spectrum from FROG; inset, retrieved temporal intensity by FROG, indicating a pulse duration of 16 fs. (b) MIR spectra with ZnSe and ZnS crystals pumped by a 1 μm laser source. The measured average powers behind the 2.7 μm long-pass filter are 0.3 and 0.5 mW, respectively.

threshold for ZnS and, especially ZnSe, at 1 μm, limiting the intensities that can be applied for the nonlinear process. Secondly, the coherence lengths for RQPM and the average crystal grain sizes are better matched for the 2 μm case, enhancing the resonance effect [20]. In contrast, the coherence lengths for a pump at 980 nm and a signal at 1080 nm are ~30 μm for both ZnS and ZnSe, which is far away from their average grain size of ~60 μm. Furthermore, the phase-mismatch vector, $\Delta k = k_3 - k_2 - k_1$, is also approximately twice as large for conversion at 1 μm. Since the intensity of the generated signal is proportional to the inverse square of Δk [20], this also contributes to the lower efficiency.

The average infrared power driven by both 1 and 2 μm sources could be further boosted in the future. Since the DFG signal has a linear variation as a function of the sample thickness under the RQPM condition [20], higher average MIR power can be expected by increasing the interaction length while maintaining the intensity. This can be achieved by using a higher power pump source, together with a larger spot size and a longer Rayleigh length. External cooling of the nonlinear crystals can also be implemented to help reduce potential thermal-induced instabilities. In addition, the DFG signal has a resonant yield when the grain size of the polycrystalline material is close to the coherence length [20,21]. In the case for ZnSe, the grain size (50–70 μm) is still somewhat smaller than the coherence length (~75 μm) when a 2 μm source is used. This can be improved through annealing [21] to obtain larger and more suitable grain sizes. Considering the higher damage threshold, lower Δk for DFG, and the average grain size of off-the-shelf polycrystalline elements, pumping at 2 μm is the preferred route over 1 μm pumping for generating MIR through RQPM with ZnS and ZnSe crystals.

Table 1. Summary of the Parameters with 1 and 2 μm Pump Sources[a]

	I_{Focus} [GW/cm^2]	P_{Pump} [W]	τ [fs]	f_{rep} [MHz]	D_{Grain} [μm]	Lc [μm]	Δk [mm^{-1}]	P_{Avg} [mW]	η [%]
1 μm ZnSe	56	4	16	28	50–70	27.3	115.2	0.5	0.02
1 μm ZnS	90	6.5	16	28	60	34.7	90.4	0.8	0.02
2 μm ZnSe	110	7	15	77	50–70	76.5	41.1	25	0.51
2 μm ZnS	110	7	15	77	60	56.6	55.5	35	0.71

[a]I_{Focus}, peak intensity in the focus; P_{Pump}, pump power; τ, pulse duration of the pump pulses; f_{rep}, repetition rate of the pump pulses; D_{Grain}, grain size; Lc, coherence length; Δk, phase-mismatch vector; P_{Avg}, average power of the MIR laser generated inside the crystal; η, conversion efficiency.

In conclusion, we report the generation of broadband MIR via cascaded intra-pulse DFG based on random quasi-phase-matching. To the best of our knowledge, this is the first time that random QPM has been used for intra-pulse DFG. It is demonstrated in commercially available ZnSe and ZnS polycrystalline materials with both 1 and 2 μm pump sources. Compared to the 1 μm source, the 2 μm source shows one order of magnitude improvement in conversion efficiency and average output power. A spectrum covering from 2.7 to 20 μm with an average power of over 16 mW can be obtained with a ZnSe crystal, and a spectral coverage from 2.7 to 15 μm with an average power of over 22 mW can be obtained with a ZnS crystal. These powers obtained by random QPM are enough to saturate typical HgCdTe detectors used for this wavelength range. The system, which uses economical and widely available polycrystalline materials, combines the robust and simple single-beam geometry for intra-pulse DFG with the extreme ease-of-use of the random quasi-phase-matched process. Moreover, intra-pulse DFG also has the potential to generate few-cycle infrared output with passive CEP stability. These advantages make this scheme highly attractive for many research applications.

Funding. Munich-Centre for Advanced Photonics (MAP).

Acknowledgment. The authors thank Dominik Bauer and Dirk Sutter from TRUMPF Laser GmbH for their support and for providing the thin-disk technology.

†These authors contributed equally to this work.

REFERENCES

1. J. Haas and B. Mizaikoff, Annu. Rev. Anal. Chem. **9**, 45 (2016).
2. A. Muraviev, V. Smolski, Z. Loparo, and K. Vodopyanov, Nat. Photonics **12**, 209 (2018).
3. G. Cinque, M. D. Frogley, and R. Bartolini, Rend. Lincei **22**, 33 (2011).
4. F. Keilmann and S. Amarie, J. Infrared Millimeter, Terahertz Waves **33**, 479 (2012).
5. C. R. Petersen, U. Møller, I. Kubat, B. Zhou, S. Dupont, J. Ramsay, T. Benson, S. Sujecki, N. Abdel-Moneim, and Z. Tang, Nat. Photonics **8**, 830 (2014).
6. P. Rauter and F. Capasso, Laser Photonics Rev. **9**, 452 (2015).
7. V. Smolski, S. Vasilyev, P. Schunemann, S. Mirov, and K. Vodopyanov, Opt. Lett. **40**, 2906 (2015).
8. S. Xie, N. Tolstik, J. C. Travers, E. Sorokin, C. Caillaud, J. Troles, P. S. J. Russell, and I. T. Sorokina, Opt. Express **24**, 12406 (2016).
9. R. Huber, A. Brodschelm, F. Tauser, and A. Leitenstorfer, Appl. Phys. Lett. **76**, 3191 (2000).
10. I. Pupeza, D. Sánchez, J. Zhang, N. Lilienfein, M. Seidel, N. Karpowicz, T. Paasch-Colberg, I. Znakovskaya, M. Pescher, and W. Schweinberger, Nat. Photonics **9**, 721 (2015).
11. T. Steinle, F. Neubrech, A. Steinmann, X. Yin, and H. Giessen, Opt. Express **23**, 11105 (2015).
12. J. Zhang, K. F. Mak, N. Nagl, M. Seidel, D. Bauer, D. Sutter, V. Pervak, F. Krausz, and O. Pronin, Light Sci. Appl. **7**, 17180 (2018).
13. C. Gaida, M. Gebhardt, T. Heuermann, F. Stutzki, C. Jauregui, J. Antonio-Lopez, A. Schülzgen, R. Amezcua-Correa, A. Tünnermann, and I. Pupeza, Light Sci. Appl. **7**, 94 (2018).
14. O. Novák, P. R. Krogen, T. Kroh, T. Mocek, F. X. Kärtner, and K.-H. Hong, Opt. Lett. **43**, 1335 (2018).
15. Q. Wang, J. Zhang, A. Kessel, N. Nagl, V. Pervak, O. Pronin, and K. F. Mak, *Advanced Solid State Lasers* (Optical Society of America, 2018), paper ATu6A.4.
16. Q. Wang, J. Zhang, A. Kessel, N. Nagl, V. Pervak, O. Pronin, and K. F. Mak, Opt. Lett. **44**, 2566 (2019).
17. S. Vasilyev, I. S. Moskalev, V. O. Smolski, J. M. Peppers, M. Mirov, A. V. Muraviev, K. Zawilski, P. G. Schunemann, S. B. Mirov, and K. L. Vodopyanov, Optica **6**, 111 (2019).
18. E. Sorokin, A. Marandi, P. G. Schunemann, M. Fejer, R. L. Byer, and I. T. Sorokina, Opt. Express **26**, 9963 (2018).
19. M. Angell, R. Emerson, J. Hoyt, J. Gibbons, L. Eyres, M. Bortz, and M. Fejer, Appl. Phys. Lett. **64**, 3107 (1994).
20. M. Baudrier-Raybaut, R. Haidar, P. Kupecek, P. Lemasson, and E. Rosencher, Nature **432**, 374 (2004).
21. Q. Ru, N. Lee, X. Chen, K. Zhong, G. Tsoy, M. Mirov, S. Vasilyev, S. B. Mirov, and K. L. Vodopyanov, Optica **4**, 617 (2017).
22. Q. Lou, J. Zhou, Y. Qi, and H. Cai, *Advances in Ceramics-Synthesis and Characterization, Processing and Specific Applications* (InTech, 2011).
23. S. Vasilyev, I. Moskalev, M. Mirov, V. Smolski, S. Mirov, and V. Gapontsev, Opt. Mater. Express **7**, 2636 (2017).
24. S. Vasilyev, I. Moskalev, V. Smolski, J. Peppers, M. Mirov, V. Fedorov, D. Martyshkin, S. Mirov, and V. Gapontsev, Optica **6**, 126 (2019).
25. J. Zhang, K. F. Mak, and O. Pronin, IEEE J. Sel. Top. Quantum **24**, 1102111 (2018).
26. J. Connolly, B. di Benedetto, and R. Donadio, Proc. SPIE **181**, 141 (1979).
27. M. Debenham, Appl. Opt. **23**, 2238 (1984).
28. K. Fritsch, M. Poetzlberger, V. Pervak, J. Brons, and O. Pronin, Opt. Lett. **43**, 4643 (2018).
29. D. Grojo, S. Leyder, P. Delaporte, W. Marine, M. Sentis, and O. Utéza, Phys. Rev. B **88**, 195135 (2013).
30. L. Gallais, D.-B. Douti, M. Commandré, G. Batavičiūtė, E. Pupka, M. Ščiuka, L. Smalakys, V. Sirutkaitis, and A. Melninkaitis, J. Appl. Phys. **117**, 223103 (2015).